Title

Paramagnetic fluorinated nanoemulsions for sensitive cellular fluorine-19 magnetic resonance imaging

Journal

Nature Materials, 15(6)

ISSN

1476-1122

Authors

Kislukhin, Alexander A

Xu, Hongyan

Adams, Stephen R

et al.

Publication Date

2016-06-01

DOI

10.1038/nmat4585

Peer reviewed

Published in final edited form as:

Nat Mater. 2016 June ; 15(6): 662–668. doi:10.1038/nmat4585.

Paramagnetic fluorinated nanoemulsions for sensitive cellular fluorine-19 magnetic resonance imaging

Alexander A. Kislukhin[1], **Hongyan Xu**[2], **Stephen R. Adams**[1], **Kazim H. Narsinh**[2], **Roger Y. Tsien**[1,3,4,*], and **Eric T. Ahrens**[2,*]

[1]Department of Pharmacology, University of California, San Diego, La Jolla, CA 92093

[2]Department of Radiology, University of California, San Diego, La Jolla, CA 92093

[3]Department of Chemistry and Biochemistry, University of California, San Diego, La Jolla, CA 92093

[4]Howard Hughes Medical Institute, University of California, San Diego, La Jolla, CA 92093

Abstract

Fluorine-19 magnetic resonance imaging (^{19}F MRI) probes enable quantitative *in vivo* detection of cell therapies and inflammatory cells. Here, we describe the formulation of perfluorocarbon-based nanoemulsions with improved sensitivity for cellular MRI. Reduction of the ^{19}F spin-lattice relaxation time (T_1) enables rapid imaging and an improved signal-to-noise ratio, thereby improving cell detection sensitivity. We synthesized metal-binding β-diketones conjugated to linear perfluoropolyether (PFPE), formulated these fluorinated ligands as aqueous nanoemulsions, and then metalated them with various transition and lanthanide ions in the fluorous phase. Iron(III) *tris*-β-diketonate ('FETRIS') nanoemulsions with PFPE have low cytotoxicity (<20%) and superior MRI properties. Moreover, the ^{19}F T_1 can readily be reduced by an order of magnitude and tuned by stoichiometric modulation of the iron concentration. The resulting ^{19}F MRI detection sensitivity is enhanced by 3-to-5 fold over previously used tracers at 11.7 T, and is predicted to increase by at least 8-fold at clinical field strength of 3 T.

Corresponding Authors: Roger Y. Tsien, PhD, Departments of Pharmacology and of Chemistry and Biochemistry, University of California, San Diego, La Jolla, CA 92093-0647, USA, Phone: (858) 534-4891, rtsien@ucsd.edu, Eric T. Ahrens, PhD, Department of Radiology, University of California, San Diego, La Jolla, CA 92093, USA, Phone: (858) 246-0279, eahrens@ucsd.edu.

Author Contributions

1. A.A.K. designed synthesis schemes, performed chemical synthesis of the molecules and emulsions, characterized synthesis products, and wrote first draft of manuscript.
2. H.X. performed tissue culture experiments.
3. S.R.A. helped designed experiments, performed chemical synthesis, and helped edit manuscript.
4. K.N. assisted with the in vivo animal experiments and MRI renderings and helped edit manuscript.
5. R.Y.T. helped design experiments and edit manuscript.
6. E.T.A. helped design experiments, acquired MRI data in phantoms and in mice, edited final version of manuscript.

Competing Financial Interests

None

Magnetic resonance imaging (MRI) is becoming a clinical tool for visualizing specific cell populations in the body[1]. MRI cell detection using exogenous agents can be used to visualize the *in vivo* trafficking and behaviour of immune or stem cells used to treat a host of diseases. Fluorine-19 (^{19}F) 'tracer' agents are an emerging approach to intracellularly label cells of interest, either *ex vivo* or *in situ*, to enable cell detection via ^{19}F MRI[1, 2]. The ^{19}F label yields positive-signal 'hot-spot' images, with no background signal due to negligible fluorine concentration in tissues. Images can be quantified to measure apparent cell numbers at sites of accumulation[2, 3], thereby enabling '*in vivo* cytometry'[4]. Tracer agent compositions have mostly focused on nontoxic perfluorocarbons (PFC). Clinical translation of ^{19}F cell detection has recently been realized in patients[5] using PFC nanoemulsion to label a dendritic cell cancer vaccine; in these experiments, the cell detection limit was conservatively estimated to be of order 10^5 cells per voxel[5].

Improving the sensitivity of ^{19}F cell detection could lower the barriers for using this technology in a wider range of biomedical applications. One approach for boosting sensitivity is by decreasing the intrinsically-high ^{19}F spin-lattice relaxation time (T_1) of PFC molecules[6–8]. The T_1 ultimately limits the rate of ^{19}F MRI data acquisitions. Often, ^{19}F images require summation of multiple acquisitions (*i.e.*, signal averaging) to generate a sufficient signal-to-noise ratio (*SNR*) for confident interpretation. High ^{19}F T_1 values require a long repetition time (TR) to allow for longitudinal signal recovery, thus limiting the number of signal acquisitions attainable during a fixed total imaging time (t_i). As t_i is constrained when scanning patients, the key parameter to maximize is $SNR/\sqrt{t_i}$. Shortening T_1 can increase $SNR/\sqrt{t_i}$, sensitivity, and decrease the minimum number of detectable cells per voxel. In practice, reducing T_1 by molecular design can also lead to a reduction in the spin-spin relaxation time (T_2) and line broadening of the resonance; this effect may degrade the *SNR* if T_2 becomes comparable to the data acquisition sampling time along the frequency encoding direction[9]. The creation of stable and cytocompatible ^{19}F agents with 'ultra-fast' T_1 is an open challenge that can greatly impact the MRI field, enabling accelerated MRI acquisitions and the detection of sparser cell populations *in vivo*.

The relaxation times T_1 and T_2 can be profoundly altered by high-spin paramagnetic metal ions (e.g., Mn^{2+}, Fe^{3+}, Gd^{3+}). Prior studies[6] have attached Gd^{3+} to the outer surface of the PFC nanoemulsion droplet resulting in modest reductions in T_1. With increasing distance (r), the steep fall-off ($\sim r^{-6}$) of paramagnetic relaxation rate enhancement from paramagnetic centers limit the efficacy of relaxation agents bound to the surface of PFC nanoparticles.[8, 10] Thus, effective relaxation enhancement necessitates introduction of metal ions into the fluorous phase, *i.e.*, within the nanoemulsion droplets, to achieve a short T_1 using a minimum amount of a paramagnetic additive.

We describe the scalable synthesis and properties of a family of paramagnetic PFC nanoemulsions with excellent ^{19}F MRI and biological properties. We show that fluorinated materials incorporating suitable ligands can tightly bind and retain sufficient amounts of metal ions in the fluorous phase of the nanoemulsion to yield ^{19}F agents with greatly enhanced sensitivity. These new nanoemulsion materials contain metal-binding β-diketones conjugated to linear perfluoropolyether (PFPE). Using these agents, we describe preliminary

assessments of the biocompatibility, cell labeling stability, and *in vivo* MRI studies in mice. Sensitivity enhancement of these materials will potentially accelerate the use of ^{19}F cell detection in a host of clinical cell therapy trials and for diagnostic inflammation imaging.

Modeling of paramagnetic relaxation enhancement

In the initial design of ^{19}F probes, we conducted magnetic resonance relaxation time modeling of the impact of dissolving metals ions into PFC. Solomon–Bloembergen–Morgan (SBM) theory[11, 12] describes paramagnetic relaxation enhancement (PRE) of $R_1=1/T_1$ and $R_2=1/T_2$ of surrounding media at a given magnetic field strength, molecular mobility, and metal concentration (See Supporting Information). Using SBM theory, we found optimal parameters for enhancement of R_1 while minimizing linewidth broadening, *i.e.*, R_2. The modeling results (Fig. S1) show that Fe^{3+} uniformly dispersed in PFC will provide the most robust enhancement of ^{19}F R_1. Mn^{2+} and Gd^{3+} are likely to cause severe line broadening due to a large increase in R_2, especially at high magnetic field strengths. This line broadening originates from very slow electronic relaxation in Mn^{2+} and Gd^{3+} (Fig. S1).

Design and preparation of metal-binding perfluorocarbons

Design of a cytocompatible fluorous-soluble metal chelate requires careful consideration. The steep fall-off of PRE with increasing distance ($\sim r^{-6}$) necessitates solubilisation of individual metal ions, as opposed to incorporating metal-bearing oligomeric clusters or nanoparticles. The metal must not efflux from the fluorous phase during cell labelling and after *in vivo* administration. The high electronegativity of fluorine imparts very low cohesive energy density[13] and Lewis basicity[14] to heavily fluorinated compounds, making them extremely poor solvents and ligands. The choice of ligands compatible with fluorous phase is therefore limited to the most hydrophobic scaffolds, with as few intermolecular interactions as possible. To maximize solubility in the fluorous phase, the resulting metal complex should be uncharged and coordinatively saturated. These criteria can be satisfied by using bidentate, monoionic ligands (**L**) that form high-spin, charge-neutral *tris*-complexes with trivalent metals (FeL_3, GdL_3) and *bis*-complexes with divalent metals (MnL_2). Of these, only FeL_3 are coordinatively saturated, due to the small size of the parent Fe^{3+} ion. Coordinatively unsaturated complexes of larger Mn^{2+} and Gd^{3+} tend to be unstable with respect to the formation of oligomeric[15], charged, or ternary complexes[16] (*e.g.*, $[GdL_3]_n$, $[GdL_4]^-$, $[GdL_3{\bullet}(H_2O)_x]$). Although gadolinium chelates are widely used contrast agents in clinical ^{1}H MRI because Gd^{3+} has the highest magnetic moment, we predict that Fe^{3+} is better suited for ^{19}F applications.

Initially, we tested the results of the PRE modeling [see Supplementary Information (SI) Fig. S1] using small molecules. Fluorinated β-diketone **H-fod** (Fig. 1) was chosen as starting point. Addition of 2.8 mM **H-fod** to the aqueous phase of a premade PFPE nanoemulsion displays apparent dissolution of the diketone and appearance of heptafluoropropyl groups in ^{19}F NMR spectra featuring three broad singlets. Addition of 0.7 mM $FeCl_3$ led to the slow formation of orange-colored $Fe(fod)_3$ and a commensurate increase in R_1 from 2.3 to 27.0 s^{-1} and in R_2 from 4.0 to 85.6 s^{-1} (at 9.4 T) of the major PFPE resonance (−91.4 ppm) by 24 hours (Fig. S3). With $GdCl_3$, lower R_1 (12.8 s^{-1}) and higher R_2 (285 s^{-1}) values were

obtained. The corresponding gadolinium complex displayed modest R_1 values accompanied by strong line broadening, a likely consequence of both high electronic relaxation time (T_{1e}) of Gd^{3+} and high rotational correlation time (τ_F) of the oligomeric gadolinium chelate (see Eqs. S1–S4 and Fig. S1 and S2 in SI). However, broad NMR signals of the ligand in the absence of metals and slow metalation kinetics suggested insufficient solubility of **H-fod** in PFPE.

To improve solubility, we investigated fluorinated β-diketones (FDK) that have a greater fluorine content. We prepared the PFPE-based ligand ***p*An-FDK** using Claisen condensation[17] between **PFPE-OMe** and excess *p*-methoxyacetophenone, yielding highly pure ***p*An-FDK** product at >10 g scale upon simple extractive workup (Fig. 2a). ^{1}H NMR analysis revealed new peaks at 6.46 and 15.35 ppm, characteristic of a diketone in enol form (Fig. S4). This ligand was used for subsequent studies.

To evaluate ^{19}F MRI properties, we blended ***p*An-FDK** with a variety of perfluorocarbon derivatives and formulated these blended oils into aqueous nanoemulsions using microfluidization. Nanoemulsions (Fig. 2c) included ***p*An-FDK** alone (emulsion **A**), or as a blend with PFPE diethylamide (DEA) (**B**), PFPE (**D**), perfluorooctyl bromide (PFOB) (**F**), or a short PFPE oligomer perfluorotetraglyme (PF4G) (**G**). Emulsions **C** (pure PFPE-DEA) and **E** (pure PFPE) are controls that cannot bind metals (Fig. 2c). We note that PFOB was tested because of its rapid clearance from the body and prior use clinically, but is not preferred for MRI cell detection due to its multiple ^{19}F resonances that diminish image quality[18]. In all formulations **A–G**, stable nanoemulsions were formed, with similar physical characteristics. Dynamic light scattering (DLS) measurements in **A–G** displayed monodisperse nanoemulsions with a polydispersity index (PDI) of <0.2 and average droplet diameters ranging from 140–200 nm and negative ζ-potentials of −27 to −56 mV (Fig. S5). No change in DLS measurements were noted for up to 8 months of storage at 4 °C. Nanoemulsion composition was confirmed by ^{19}F NMR (Fig. 2d). Terminal CF_2 atoms of PFPE derivatives have resonances between −70 and −85 ppm. Presence of only one major peak in this spectral range in single-component emulsions **A** and **C** confirmed high purities of the starting oils; emulsion **B** shows peaks from both components in the expected 1:1 ratio. Core CF_2CF_2O units resonating at −91 ppm comprise ~90% of the total ^{19}F spectral weight and is typically the only signal detectable by ^{19}F MRI, which generally has a much lower SNR compared to conventional ^{1}H images.

Properties of metalated nanoemulsions

The Pluronic surfactant used in the nanoemulsion formulation is permeable to ions enabling direct metalation of FDK nanoemulsions by the addition of metal chloride into the aqueous phase (Fig. 2e). Optical changes due to the formation of metal complexes were readily observed (Fig. 2f and S6). Among these, europium chelates are notable for their bright photoluminescence which may be useful for studying intracellular localization and trafficking of the PFC droplets (Fig. S11e). Importantly, addition of $FeCl_3$ caused rapid (k_{obs} = 0.69±0.10 min^{-1}) appearance (Fig. S7) of characteristic charge transfer bands of ferric diketonates[19] (ε_{390} =23, ε_{500}=4.9 $mM^{-1}cm^{-1}$) that linearly increased in intensity with increasing [Fe^{3+}] until the Fe:FDK ratio of *ca.* 1:3 was reached, consistent with ferric *tris*-

diketonate (Fig. 2f). Henceforth, the term 'FETRIS' (FErric *TRIS*-diketonate) refers to ***p*An-FDK** blended with PFPE and metalated with Fe^{3+}.

Relaxometric evaluation of nanoemulsions in the presence of different metals (Fig. 3a) revealed that binding of Fe^{3+} resulted in modest line broadening of all ^{19}F NMR resonances, including the main PFPE peak at −91 ppm. The highest R_1 observed (158.2±2.5 s^{-1} at 11.7 T), with a linewidth of 4 kHz, was with FETRIS saturated with Fe^{3+}. Despite the largest number of unpaired electrons, Gd^{3+} showed a two-fold lower R_1 compared to Fe^{3+}, with severe line broadening. Mn^{2+} gave moderately broad signals with the lowest R_1 of the triad. To confirm that the linewidth of metalated nanoemulsions is dominated by paramagnetism and not by metal binding *per se*, diamagnetic Ga^{3+}, with a similar ionic radius to Fe^{3+}, was included in the analysis and was found to have R_1 and R_2 equal to 2.08±0.01 s^{-1} and 20.9 ± 0.3 s^{-1}, respectively. Also, the small change in relaxation rates relative to the unmetalated emulsion, with R_1 = 2.37±0.01 s^{-1}, and R_2 = 15.1±0.2 s^{-1} (9.4 T), is attributable to an increase in the effective molecular weight upon formation of the metal complex.

We determined the phase distribution of the paramagnetic ions and the metal binding capacity of FDK nanoemulsions (Fig. 3b). Measurement of R_1 at 11.7 T for both PFPE (fluorous phase) and trifluoroacetate reference (TFA) added to the aqueous phase revealed that nanoemulsions efficiently extracted Gd^{3+} and Fe^{3+} from water into the fluorous phase. R_1 of PFPE reached a plateau at ligand-to-metal ratio of *ca.* 2.5; increasing metal concentration further affected the R_1 of TFA. Notably, an increase in R_1 of TFA was observed even at the lowest Gd^{3+} concentration in pure PFPE nanoemulsion, confirming that the paramagnetic ion stays in the aqueous phase. We speculate that the modest (~2-fold) increase in R_1 of PFPE in this case was likely due to binding of Gd^{3+} ions to the nanoemulsion surface[8, 10]. We observed a divergent field and temperature dependence of R_1 and R_2 in FETRIS nanoemulsions (Fig 3c,d, Fig. S8). Further control over relaxation parameters was achieved by tuning molecular weight and viscosity of the emulsion components (Fig. S9). Other rare earths had only a minor effect on R_1, consistent with fast electronic relaxation in these metal ions[20] (Fig. S10).

We also evaluated the stability of metal–FDK complexes. Using metal-loaded nanoemulsion, we monitored changes in photoluminescence (Eu^{3+}) and absorbance (Fe^{3+}) in the presence of excess competing ligands to study potential leakage of metal from the fluorous phase. Ethylenediaminetetraacetate (EDTA), a strong metal chelator[21], rapidly (<5 min) abolished the photoluminescence of europium-loaded emulsion due to complete sequestration of Eu^{3+} to the aqueous phase to form a non-photoluminescent EDTA complex. In contrast, FETRIS nanoemulsion showed no decrease in characteristic absorbance of the Fe^{3+} chelate, even with prolonged exposure to EDTA. To estimate long-term stability of FETRIS nanoemulsions, relaxation rates were measured in the presence of EDTA (Fig. 4). PFPE-based nanoemulsion showed <20% decrease in R_1 over 2 weeks of incubation at 37 °C with EDTA.

Next, we examined FETRIS nanoemulsion properties in labeled cells. *Ex vivo* labeling of a rodent glioma cell line (GL261) with FETRIS showed good viability post-labeling (Fig. 5a), with loadings on the order of ~10^{12} ^{19}F atoms/cell (Fig. 5b). Uptake of FETRIS was evident

by the orange color of cell pellets, and optical absorbance in the lysate correlated with the ^{19}F content determined by NMR (Fig. 5c). Fluorine-19 relaxometry of labeled cells (Fig. S11) showed that FETRIS nanoemulsion did not appear to lose Fe^{3+} to the intracellular milieu over time; moreover, in the same nanoemulsion formulated without added Fe^{3+}, it did not appear to sequester endogenous Fe^{3+} from the cell's labile iron pool (Fig. S11c). However, Gd^{3+} substituted for Fe^{3+} in the nanoemulsion displayed evidence of some metal leakage upon cell labeling; we observed *ca.* 25% reduction of ^{19}F R_1 values after labeling (Fig. S11d).

Magnetic resonance imaging with FETRIS

Phantom ^{19}F MRI studies demonstrated the feasibility of imaging FETRIS using conventional MRI methods. A phantom sample was prepared consisting of two NMR tubes containing FETRIS prepared with parameters R_1/R_2=32.5/170 s^{-1} and the same emulsion without metal (R_1/R_2=2.2/3.7 s^{-1}); tubes were embedded in agarose. Images were acquired at 11.7 T using a spin-density weighted gradient echo (GRE) sequence, with scanning parameters set at the Ernst angle condition[9] for optimal imaging of the FETRIS specimen, and a ~4 min image acquisition time. Figure 6a displays phantom MRI results, where the FETRIS sample appears hyperintense; the measured ^{19}F image SNR for FETRIS and Fe-negative specimens were 8.6 and 1.7, respectively, yielding a SNR improvement of ~5 for the FETRIS sample, without Rician correction for low SNR regime[3]. If each capillary was imaged using its appropriate Ernst angle, the SNR improvement would be ~3.3 (see modeling results Fig. S12). To further minimize potential T_2 signal loss when imaging FETRIS agents, one could potentially use so called Ultrashort TE (UTE) or Zero TE (ZTE) pulse sequences[7]. Pulse sequences like GRE are commonplace on clinical scanners, whereas ZTE is not yet readily provided by MRI vendors.

Preliminary *in vivo* imaging of FETRIS-labeled cells was performed. Glioma cells were labeled with FETRIS nanoemulsion (50 wt.% ***p*An-FDK**, 50 wt.% **PFPE**) *ex vivo* to a level of ~10^{12} ^{19}F/cell. A second batch of glioma cells was labeled at comparable levels with PFPE emulsion without metal. Cells (5×10^6 per side) were injected subcutaneously into left (no metal) and right (FETRIS) flanks in syngeneic C57BL/6 mice (N=3). After 24 hours, mice were imaged with $^{1}H/^{19}F$ MRI at 11.7T (Fig. 6b). The ^{19}F images were acquired using a three-dimensional ZTE sequence (Fig. 6b). Cells were readily visible (SNR~7) in the right injected flank (Fig. 6b), but not on the left side (no metal). Future *in vivo* studies will utilize FETRIS to image stem cells and immune cell populations in preclinical models.

Outlook

Here we present a unique approach for formulating nanoemulsions using PFPE-based β-diketones (FDK) as metal chelators. These ligands have previously been studied in the context of material science[16], NMR spectroscopy[22], and catalysis[23]. We show that FDK is well-suited for incorporating large amounts of paramagnetic metal ions into the fluorous liquids. Formulated as stable PFPE-in-water nanoemulsions, FDK efficiently and irreversibly extract Fe^{3+} ions from aqueous solution into the fluorous phase, giving rise to cytocompatible FETRIS agent. These paramagnetic materials are useful for ^{19}F MRI with

enhanced sensitivity due to a dramatic reduction in T_1, a fundamental parameter limiting the speed of MRI data acquisitions. The ^{19}F T_1 value reduction is magnetic field-strength dependent, but can potentially be accelerated to values approaching 80× at clinical field strengths, yielding a >8-fold sensitivity increase in ^{19}F detection (Fig. S12). These sensitivity increases diminish at higher magnetic field strengths (Fig. S12). We show that FETRIS is effective for ^{19}F MRI using conventional MRI pulse sequences.

Gd^{3+} and Fe^{3+} are at the heart of T_1- and T_2-based ^1H contrast agents, respectively, but for ^{19}F MRI, the roles of these metal ions are reversed. Fe^{3+} was the optimal T_1 enhancer for perfluorocarbons, while analogous gadolinium (and manganese) chelates caused severe line broadening, essentially becoming ^{19}F T_2 agents. Paramagnetic relaxation enhancement has been previously applied to ^{19}F nuclei[7, 20, 24, 25]. ^{19}F MR probes based on macrocyclic lanthanide complexes with fluorinated substituents has been described[7, 20]. However, these paramagnetic ^{19}F tracers are not ideal for cell detection purposes. The relatively low ^{19}F content of osmotically active macrocyclic chelates makes it difficult to reach MR-detectable cell loadings compared to highly-fluorinated PFC oils. In other approaches, Gd macrocyclic chelates bound to nanoemulsion surface can be used to provide a modest enhancement of ^{19}F T_1, but these are unstable in the intracellular milieu, especially if they traffic to low pH compartments[28], which tends to separate the chelate from nanoemulsion droplet, thereby limiting long-term enhancement. In contrast, FETRIS complexes are characterized by very small rates of metal leakage even in the presence of EDTA *in vitro* and after cell labelling. The toxicity testing of FETRIS as reported here is viewed as preliminary; more rigorous *in vitro* cell studies, as well as animal testing, are needed to determine potential suitability for clinical trials. We note that emerging ^1H MRI techniques like PARACEST[26] and highly shifted proton MRI[27] have shown promise to detect multiple cell populations on standard MRI instrumentation with high specificity.

Overall, ^{19}F MRI cell detection using PFC tracer agents is a rapidly emerging alternative to ^1H-based approaches using metal-ion-based contrast agents. The technical barriers associated with implementation of ^{19}F MRI on a clinical scanner are surmountable, and clinical ^{19}F cell detection has recently been demonstrated[5]. Future improvements in sensitivity of the probes will only accelerate adoption of this technology and open up new uses for this technology; towards this goal, the excellent stability and unique magnetic properties of FETRIS should advance this field.

Methods

Emulsion preparation

The fluorocarbon oil blends were prepared from **PFPE, PFPE-DEA** (Exfluor, Round Rock, TX), **PFOB** (Acros, Pittsburgh, PA), and ***p*An-FDK** (see SI, Supplementary Methods for synthetic procedures) agents. Proportions (Fig. 2) were prepared gravimetrically in a 15 or 50 mL conical Falcon tube (Corning). Per 1 gram of PFC blend, 0.5 mL aqueous solution of Pluronic F68 (100 g/L) was added, and the mixture was vortexed at the highest speed. Water (8.5 mL) was added, followed by brief vortexing and ultrasonication (Omni Ruptor 250W, 30% power, 2 minutes, Omni International, Kennesaw, GA). The crude emulsion thus obtained was passed 4–6 times through LV1 microfluidizer (Microfluidics, Westwood, MA)

operating at 20,000 psi and filtered through a 0.2 μm Supor membrane (Pall Corp. #4187, Port Washington, NY) into sterile glass vials.

NMR measurements

NMR spectra were obtained on Magritek Spinsolve (1.0 T), Bruker Avance 300 (7.0 T), Bruker Ascend 400 (9.4 T), Jeol ACA 500 (11.7 T), and Bruker DRX-600 (14.1 T) instruments. ^{19}F NMR spectra of aqueous nanoemulsions were referenced to an internal standard (0.1 wt.% CF_3CO_2Na/D_2O, −76.00 ppm), which served as integration reference for quantitative NMR (see SI). Relaxation measurements were performed using a standard inversion recovery (with TI from 3^{-2} to 3^9 ms) pulse sequence and a Carr-Purcell-Meiboom-Gill sequence with TE values in 12 linear increments. R_1 and R_2 were obtained by non-linear fitting in MNova 6.0.2 software (Mestrelab, Escondido, CA). Fit errors were less than 5% for R_1 and 10% for R_2.

Cell labeling

Rat 9L or mouse GL261 glioma cells ($3–5\times10^6$, ATCC, Manassas, VA) were plated in 10 cm dishes and allowed to attach overnight. Immediately before cell labeling, FDK (**B** or **D**) or control (**C** or **E**) emulsion (0.5 mL) was mixed with freshly prepared $FeCl_3$ (50 mM in H_2O, 0.12 mL), protamine sulfate (1% in H_2O, 0.02 mL), and Tris base (1 M in H_2O, 0.25 mL). The dark-orange liquid was diluted to the desired PFPE content with DMEM (9L) or RPMI-1640 (GL261) media supplemented with 10% (v/v) fetal bovine serum (FBS). Labeling medium was added to cells at 5 mL/dish. After 16 h incubation at 37 °C, the cell labeling medium was removed, and cells were washed three times with phosphate buffered saline (PBS), detached by trypsinization, washed again in PBS, and resuspended in 1 mL of PBS. A portion of the cell suspension (~1/10) was used for cell number estimates by Cell Titer Glo (Promega, Madison, WI) or using a Countess II FL Cell Counter (Life Technologies, Carlsbad, CA). To assay nanoemulsion uptake, cells were pelleted and resuspended in 0.1 mL of lysis solution (0.5% Triton X, 100 mM NaCl, 20 mM Tris). A portion of this solution (6 μL) was used for absorbance measurements on NanoDrop 2000 spectrophotometer (Thermo Scientific, Pittsburgh, PA). The remainder was transferred to a 5 mm NMR tube, mixed with 0.15 mL of 0.1 wt.% CF_3CO_2Na/D_2O reference compound and ^{19}F NMR spectra were obtained to measure ^{19}F uptake, as previously described[29].

MRI

A phantom sample was prepared using 5 mm NMR tubes containing FETRIS (4.5 g/L ^{19}F, 0.5 mM Fe^{3+}, R_1/R_2 = 32.5/170 s^{-1}) and nanoemulsion without metal (R_1/R_2 = 2.2/3.7 s^{-1}); tubes were embedded in agarose. All images were acquired using a Bruker 11.7T BioSpec using a ^{19}F/^{1}H double tuned volume coil. For ^{19}F, a gradient echo (GRE) pulse sequence was used with parameters: TR/TE=15/0.83 ms (TR=recovery time), NA=256 (NA=number of averages), FOV=4×4 cm (FOV=field of view), 64×64 matrix, 8 mm thick slices, and a ~4 min data acquisition time. In this image, the echo time (TE) parameter was minimized to 0.83 ms, but at this value there is a residual amount of signal attenuation from T_2-effects in the FETRIS material (estimated ~12%). We used the Ernst angle condition[9] for optimal ^{19}F imaging of the FETRIS phantom. For ^{1}H, the GRE parameters were TR/TE=150/2 ms,

NA=8, FOV=4×4 cm, 256×256 matrix, and 2 mm slices. The ^{19}F image data was rendered in hot-iron pseudo-color using ImageJ software (NIH) and overlaid onto the grayscale ^{1}H image. For *in vivo* mouse studies, mouse GL261 glioma cells were labeled with FETRIS nanoemulsion (50 wt.% ***p*An-FDK**, 50 wt.% **PFPE**) *ex vivo* to a level of ~10^{12} ^{19}F/cell. A second batch of cells was similarly labeled but with unmetalated nanoemulsion. Cells (5×10^{6} per side) were injected subcutaneously into flanks in female syngeneic C57BL/6 mice (8–10 weeks old, N=3) using a vehicle of 0.2 ml Matrigel (BD Biosciences, Franklin Lakes, NJ) in PBS. The FETRIS labeled cells, and cells labeled with unmetalated nanoemulsion, were injected into the right and left sides, respectively. After 24 hours, mice were imaged using a three-dimensional ZTE sequence with parameters TR= 4 ms, receiver bandwidth 40 kHz, acquisition window 0.8 ms, number of projections 13030, NA=26, acquisition time 23 min, FOV=6×6×6 cm, and matrix size 64×64×64. Proton data were acquired using a two-dimensional spin-echo sequence with TR/TE=1500/14 ms, FOV=6×6 cm, and 256×256 matrix. ^{19}F data were imported into Amira software (FEI, Hillsboro, OR) and rendered in color and a grayscale slice from the ^{1}H data was embedded for anatomical display purposes.

Supplementary Material

Refer to Web version on PubMed Central for supplementary material.

Acknowledgments

This work was funded by the National Institutes of Health grants T32-CA121938 (UCSD Cancer Therapeutics Training Program, A.A.K.), R01-CA158448 (R.Y.T.), R01-EB017271 (E.T.A.), Radiological Society of North America grant RR1452 (K.H.N), and the California Institute for Regenerative Medicine grant LA1-C12-06919 (E.T.A.). We thank Mr. Toan C. Nguyen, Dr. Michael J. Patrick, Prof. Alan Waggoner, Dr. Anthony Mrse, Dr. Tatiana Didenko, Dr. Patrick McConville and Prof. Kurt Wuthrich for technical assistance, and Ms. Veronica Kislukhin for helpful discussions.

References

1. Ahrens ET, Bulte JWM. Tracking immune cells in vivo using magnetic resonance imaging. Nat Rev Immunol. 2013; 13:755–763. [PubMed: 24013185]
2. Ahrens ET, Flores R, Xu HY, Morel PA. In vivo imaging platform for tracking immunotherapeutic cells. Nat Biotechnol. 2005; 23:983–987. [PubMed: 16041364]
3. Srinivas M, Morel PA, Ernst LA, Laidlaw DH, Ahrens ET. Fluorine-19 MRI for visualization and quantification of cell migration in a diabetes model. Magn Reson Med. 2007; 58:725–734. [PubMed: 17899609]
4. Srinivas M, et al. In vivo cytometry of antigen-specific T cells using 19F MRI. Magn Reson Med. 2009; 62:747–753. [PubMed: 19585593]
5. Ahrens ET, Helfer BM, O'Hanlon CF, Schirda C. Clinical cell therapy imaging using a perfluorocarbon tracer and fluorine-19 MRI. Magn Reson Med. 2014; 72:1696–1701. [PubMed: 25241945]
6. Neubauer AM, et al. Gadolinium-modulated F-19 signals from perfluorocarbon nanoparticles as a new strategy for molecular imaging. Magn Reson Med. 2008; 60:1066–1072. [PubMed: 18956457]
7. Schmid F, Höltke C, Parker D, Faber C. Boosting 19F MRI—SNR efficient detection of paramagnetic contrast agents using ultrafast sequences. Magn Reson Med. 2013; 69:1056–1062. [PubMed: 22628001]
8. de Vries A, et al. Relaxometric studies of gadolinium-functionalized perfluorocarbon nanoparticles for MR imaging. Contrast Media Mol I. 2014; 9:83–91.

9. Brown, RW.; Cheng, YCN.; Haacke, EM.; Thompson, MR.; Venkatesan, R. Magnetic Resonance Imaging: Physical Prinicples and Sequence Design. 2nd. Hoboken, NJ: John Wiley & Sons; 2014. Edn
10. Hu L, Zhang L, Chen J, Lanza GM, Wickline SA. Diffusional mechanisms augment the fluorine MR relaxation in paramagnetic perfluorocarbon nanoparticles that provides a "relaxation switch" for detecting cellular endosomal activation. J Magn Reson Imaging. 2011; 34:653–661. [PubMed: 21761488]
11. Solomon I. Relaxation processes in a system of two spins. Phys Rev. 1955; 99:559–565.
12. Bloembergen N, Morgan LO. Proton relaxation times in paramagnetic solutions. Effects of electron spin relaxation. J Chem Phys. 1961; 34:842–850.
13. Marchionni G, Ajroldi G, Righetti MC, Pezzin G. Molecular interactions in perfluorinated and hydrogenated compounds: Linear paraffins and ethers. Macromolecules. 1993; 26:1751–1757.
14. Lai C-Z, Reardon ME, Boswell PG, Bühlmann P. Cation-coordinating properties of perfluoro-15-crown-5. J Fluor Chem. 2010; 131:42–46. [PubMed: 22180663]
15. Shibata S, Onuma S, Inoue H. Crystal and molecular structure of trimeric bis(acetylacetonato)manganese(II). Inorg Chem. 1985; 24:1723–1725.
16. Binnemans, K. Handbook on the Physics and Chemistry of Rare Earths. Karl, J-CGB.; Gschneidner, A.; Vitalij, KP., editors. Vol. 35. Elsevier; 2005. p. 107-272.
17. Barkley LB, Levine R. The synthesis of certain ketones and α-substituted β-diketones containing perfluoroalkyl groups. J Am Chem Soc. 1953; 75:2059–2063.
18. Janjic JM, Ahrens ET. Fluorine-containing nanoemulsions for MRI cell tracking. Wiley Interdisciplinary Reviews. Nanomedicine and Nanobiotechnology. 2009; 1:492–501. [PubMed: 19920872]
19. Lintvedt RL, Kernitsky LK. Ligand field information from charge-transfer spectra of substituted tris(1,3-diketonato)iron(III) chelates. Spectrochemical series for 1,3-diketones. Inorg Chem. 1970; 9:491–494.
20. Funk AM, Fries PH, Harvey P, Kenwright AM, Parker D. Experimental measurement and theoretical assessment of fast lanthanide electronic relaxation in solution with four series of isostructural complexes. J Phys Chem A. 2013; 117:905–917. [PubMed: 23259577]
21. Nash KL, Brigham D, Shehee TC, Martin A. The kinetics of lanthanide complexation by EDTA and DTPA in lactate media. Dalton T. 2012; 41:14547–14556.
22. Sanders JKM, Hanson SW, Williams DH. Paramagnetic shift reagents. Nature of the interactions. J Am Chem Soc. 1972; 94:5325–5335.
23. Lo JC, Gui J, Yabe Y, Pan C-M, Baran PS. Functionalized olefin cross-coupling to construct carbon–carbon bonds. Nature. 2014; 516:343–348. [PubMed: 25519131]
24. Harvey P, Kuprov I, Parker D. Lanthanide complexes as paramagnetic probes for 19F magnetic resonance. Eur J Inorg Chem. 2012:2015–2022.
25. De Luca E, et al. Characterisation and evaluation of paramagnetic fluorine labelled glycol chitosan conjugates for F-19 and H-1 magnetic resonance imaging. J Biol Inorg Chem. 2014; 19:215–227. [PubMed: 23955558]
26. Ferrauto G, Castelli DD, Terreno E, Aime S. In vivo MRI visualization of different cell populations labeled with PARACEST agents. Magn Reson Med. 2013; 69:1703–1711. [PubMed: 22837028]
27. Schmidt R, et al. Highly shifted proton MR imaging: Cell tracking by using direct detection of paramagnetic compounds. Radiology. 2014; 272:785–795. [PubMed: 24852443]
28. Kok MB, et al. Quantitative H-1 MRI, F-19 MRI, and F-19 MRS of cell-internalized perfluorocarbon paramagnetic nanoparticles. Contrast Media Mol Imaging. 2011; 6:19–27. [PubMed: 20648660]

References

29. Janjic JM, Srinivas M, Kadayakkara DKK, Ahrens ET. Self-delivering nanoemulsions for dual fluorine-19 MRI and fluorescence detection. J Am Chem Soc. 2008; 130:2832–2841. [PubMed: 18266363]

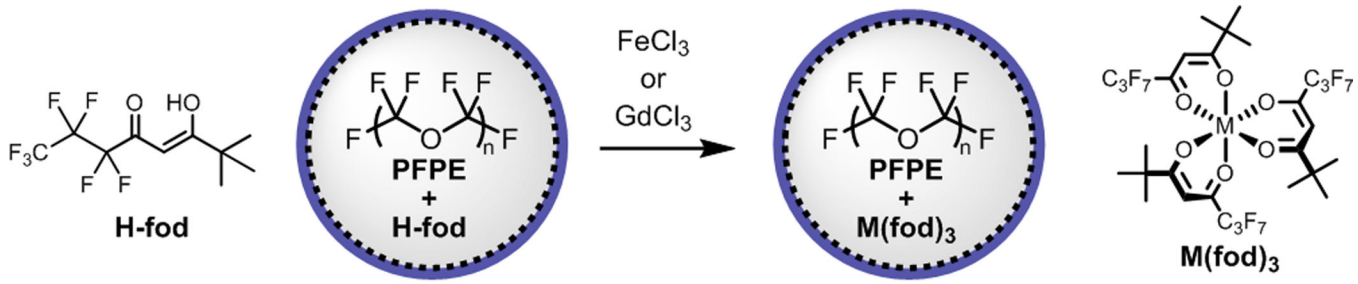

metal (M)	none	Fe	Gd
R_1 (s^{-1})	2.28±0.01	27.0±0.1	12.8±0.2
R_2 (s^{-1})	4.01±0.03	85.6±0.2	285±3
R_2/R_1	1.8	3.2	22

Figure 1. Comparison of iron and gadolinium diketonates (H-fod) as ^{19}F relaxation agents for PFPE

The relaxometry results (9.4 T) are displayed for PFPE emulsions (120 g/L PFPE) containing H-fod (2.8 mM) 24 hours after the addition of 0.7 mM metal ions. R_1 and R_2 values are reported for the main PFPE peak at −91.4 ppm. The results show that Fe^{3+} is a more effective R_1 agent than Gd^{3+}.

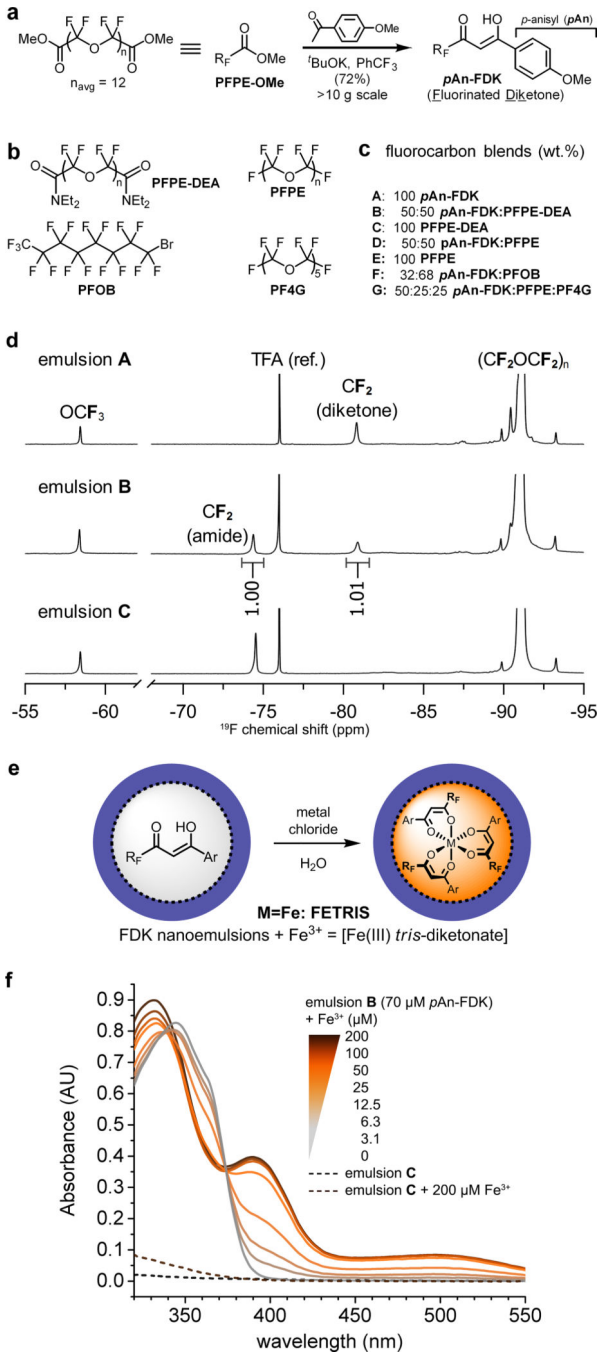

Figure 2. Preparation and characterization of metal-binding nanoemulsions for ^{19}F MRI

a, Synthesis of metal-binding fluorinated diketones (**FDK**) from **PFPE-OMe** (denoted as R_FCO_2Me). **b**, Structures of fluorocarbons used for ^{19}F MRI. **c**, Composition and preparation of various metal-binding (**A, B, D, F, G**) and control (**C, E**) fluorocarbon nanoemulsions. **d**, ^{19}F NMR spectra (11.7 T) of emulsions **A–C** (4.5 g/L ^{19}F, 90% D_2O). Signals from terminal CF_2 of diketone ligands are well separated from other peaks and are used to determine ligand concentration. The peak at −76 ppm is the reference (CF_3CO_2Na, TFA). **e**, Addition of aqueous metal chlorides to FDK emulsions yields metalated emulsions;

Ar = *p*An. **f**, Absorption spectra of metal-binding emulsion **B** (70 μM diketone, 0.09 g/L ^{19}F) (color) and control emulsion **C** (0.09 g/L) (---) in the presence of Fe^{3+}. Increasing [Fe^{3+}] causes the appearance of ferric *tris*-diketonate charge transfer bands at 395 and 500 nm that grow linearly in intensity until the *ca.* 3:1 ligand:Fe ratio is reached at 25 μM Fe^{3+}.

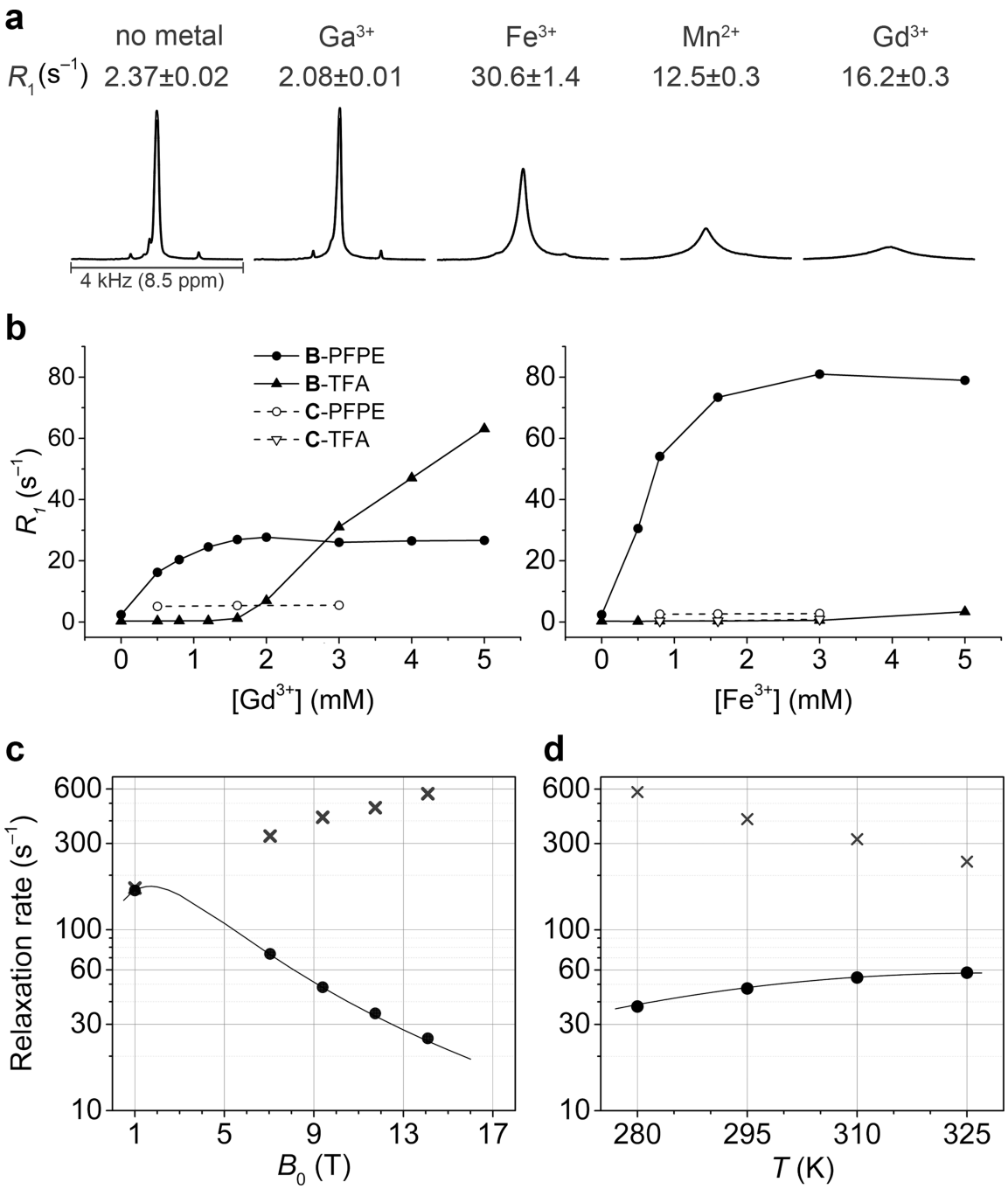

Figure 3. Fluorine-19 relaxometry of metalated PFPE emulsions

a, R_1 and ^{19}F NMR spectra of FETRIS nanoemulsion (4.5 g/L ^{19}F, 3.5 mM diketone) in the presence of 0.5 mM metal ions, 15 mM HEPES, and at pH 7.4. The peaks from different ^{19}F spectra are scaled to the same absolute intensity. **b**, Relaxometric analysis of Fe^{3+} and Gd^{3+} binding capacity. Shown are measurements of R_1 for both PFPE (fluorous phase) and trifluoroacetate reference (TFA) added to the aqueous phase. **c**, Magnetic field dependence at T = 295 K and **d**, temperature (B_0 = 9.4 T) dependence of observed relaxation rates R_1 (●) and R_2 (**x**) in FETRIS nanoemulsion (22.5 g/L ^{19}F, 17.5 mM diketone, 2.8 mM Fe^{3+})

and predicted R_1 (—) values using Eqs. S1–S4. Predicted R_1 values represent best fit to SBM equations, with r = 1.19 nm, τ_F (295 K) = 0.80 ns, τ_V (295 K) = 3.59 ps, the Arrhenius temperature dependence with activation energies of 3.6 kcal/mol for τ_F and 4.5 kcal/mol for τ_V. The diamagnetic contributions to R_1 are presumed to be negligible and Δ fixed at 0.2 cm^{-1}. R_1 values increase, while R_2 values decrease, at lower magnetic field strengths, suggesting that there will be no degradation of SNR at clinical fields due to line broadening.

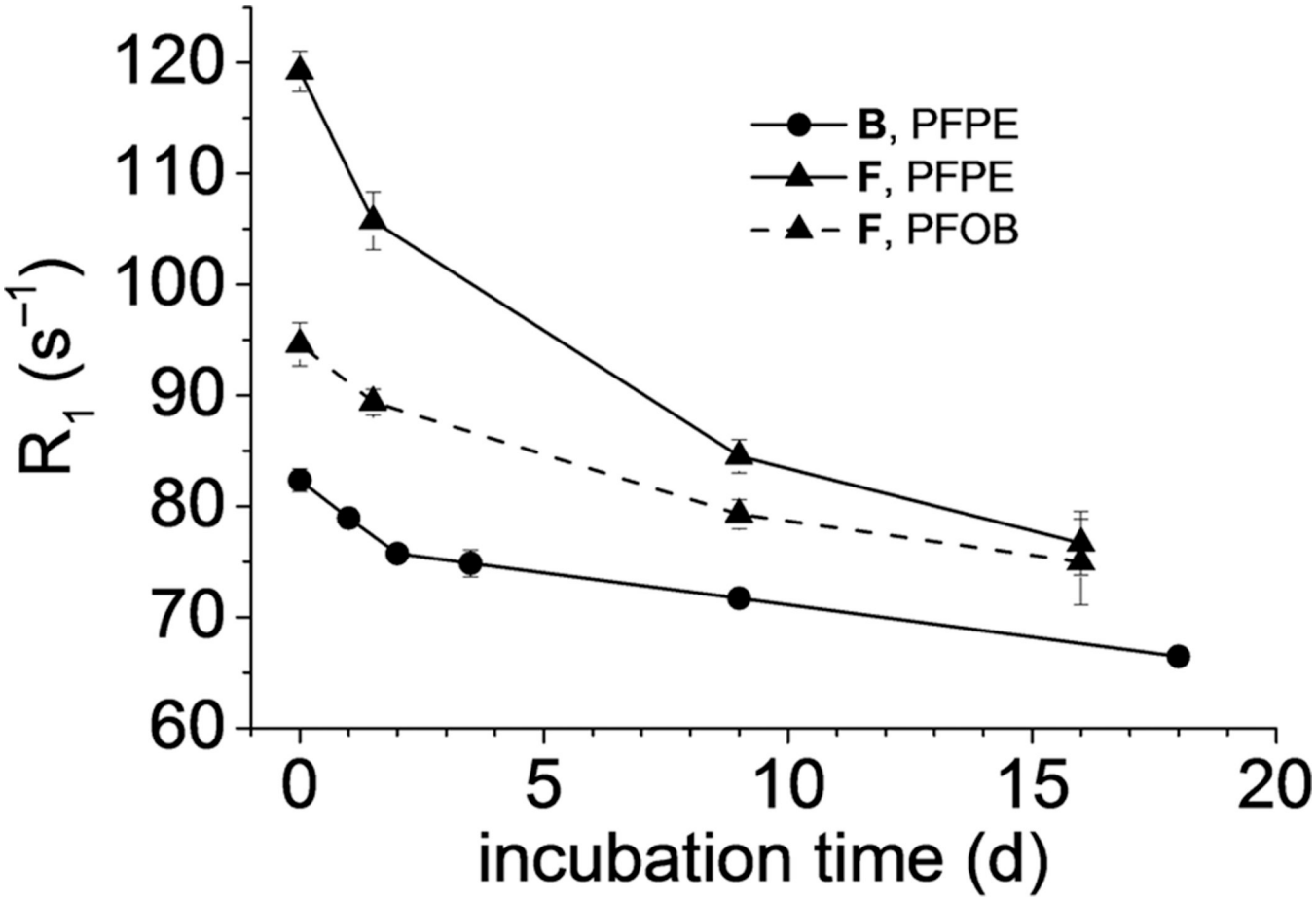

Figure 4. Relaxometry stability of FETRIS nanoemulsions in the presence of competing aqueous ligand

Nanoemulsion **B** and **F**, both metalated with 0.7 mM Fe^{3+}, were treated at 37 °C with 75 mM EDTA dissolved in aqueous phase. Shown are R_1 values of PFPE (—●—) in nanoemulsion **B**, and values for blend nanoemulsion **F**, including PFPE components (—▲—) and the CF_3 signal of PFOB (– –▲– –). A slight decrease over time is observed, as slow Fe^{3+} efflux occurs from the fluorous phase and irreversibly binds to EDTA. Error bars are standard deviations from three independent replicates.

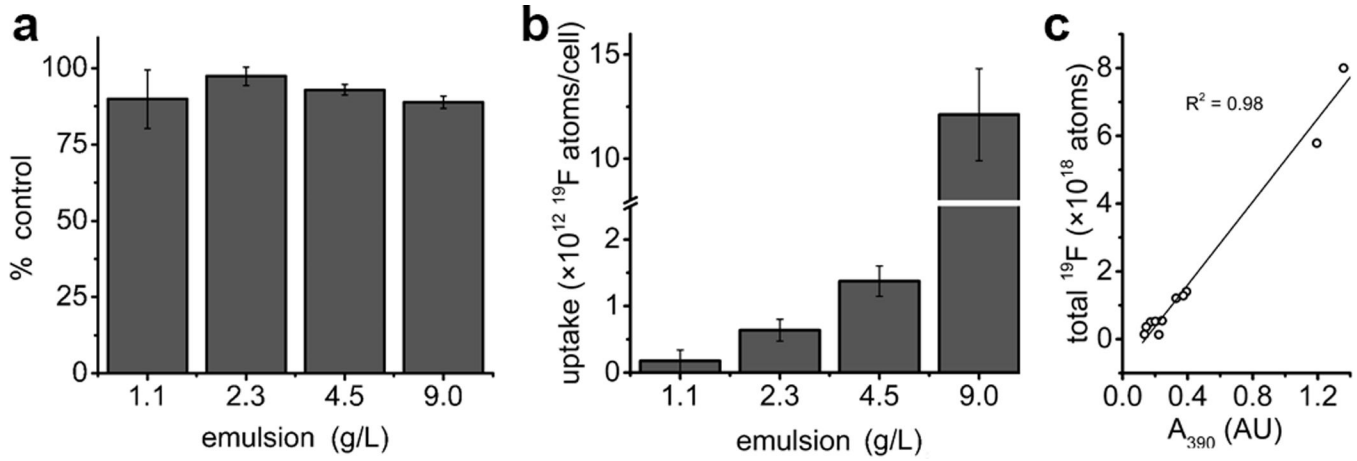

Figure 5. Cell labeling with FETRIS nanoemulsion

Cells (GL261) were labeled in culture using FETRIS nanoemulsion. **a**, Cell viability. **b**, Cell uptake of FETRIS as measured by ^{19}F NMR. **c**, Correlation of uptake determined by ^{19}F NMR with optical absorbance of cell lysate at 390 nm due to FETRIS. Error bars are standard deviations from three independent replicates.

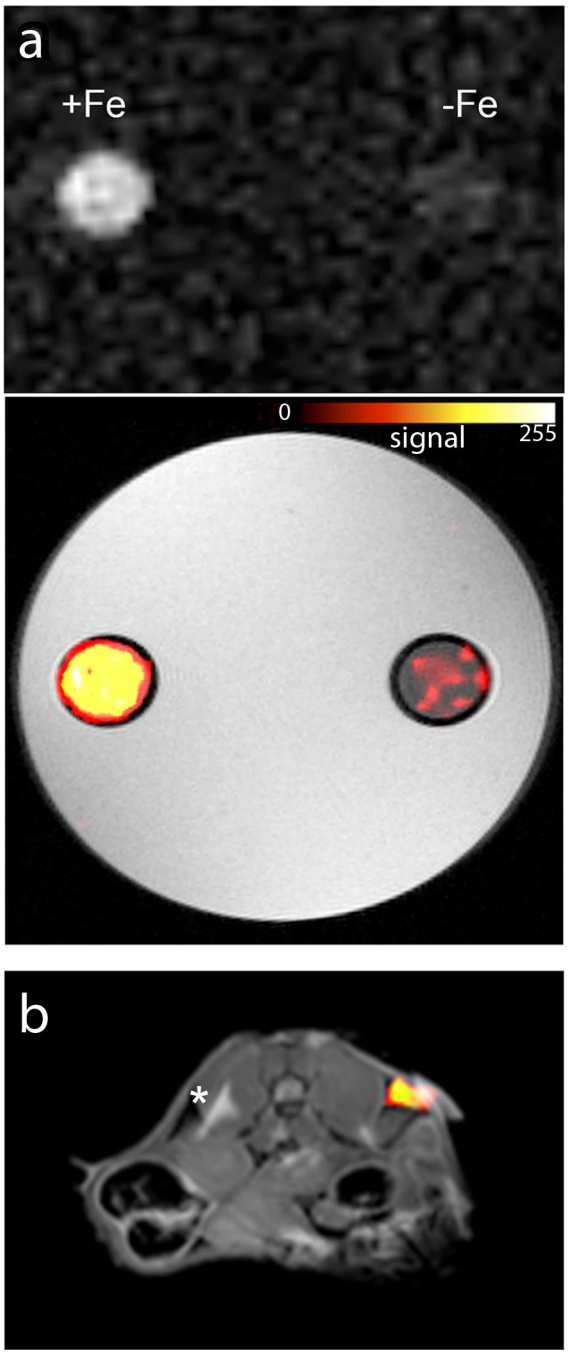

Figure 6. MRI of FETRIS nanoemulsion

a. Phantom comprised of two agarose-embedded NMR tubes containing FETRIS nanoemulsion (4.5 g/L ^{19}F) with 0.5 mM Fe^{3+} (R_1/R_2 = 32.5/170 s^{-1}) and nanoemulsion without metal (R_1/R_2 2.2/3.7 s^{-1}), denoted +Fe and −Fe, respectively. The top panel shows unthresholded ^{19}F images, and below, the ^{19}F image is thresholded, rendered in hot-iron pseudo-color (scale bar), and overlaid onto the grayscale ^{1}H image. The ^{19}F/^{1}H MRI data were acquired using a GRE sequence. **b**, Displays mouse GL261 glioma cells (5×10^6) labeled with FETRIS nanoemulsion *ex vivo* and injected subcutaneously into mouse flank.

The ^{19}F data is rendered in pseudo-color and placed on a grayscale slice from the ^{1}H data. After 24 hours, mice were imaged, and a cell 'hot-spot' is seen on the right flank in the axial view. Cells labeled with metal-free nanoemulsion and injected on the contralateral side could not be detected. Asterisk is adjacent chemical shift displacement artifact from hyperintense subcutaneous fat at 11.7T. The ^{19}F and ^{1}H images were acquired using ZTE and GRE pulse sequences, respectively. For display, a co-registered 2D GRE slice was embedded into a 3D rendering of the ^{19}F data.